Marker-free coselection for successive rounds of prime editing in human cells

Sébastien Levesque[1,2], Diana Mayorga[1,2], Jean-Philippe Fiset[1,2], Claudia Goupil[1,2], Alexis Duringer[1,2], Andréanne Loiselle[1,2], Eva Bouchard[1,2], Daniel Agudelo[1,2], Yannick Doyon[1,2*]

[1]Centre Hospitalier Universitaire de Québec Research Center - Université Laval, Québec, QC, G1V 4G2, Canada.
[2]Université Laval Cancer Research Centre, Québec, QC, G1V 0A6, Canada.

[*]Correspondence:
Yannick Doyon, Ph.D.
Centre de recherche du CHU de Québec – Université Laval
2705, boulevard Laurier, T-3-67
Québec, QC G1V 4G2
CANADA

Tel: 418-525-4444 ext. 46264
e-mail: Yannick.Doyon@crchudequebec.ulaval.ca
ORCID 0000-0002-3889-9563

ABSTRACT

Prime editing enables the introduction of precise point mutations, small insertions, or short deletions without requiring donor DNA templates. However, editing efficiency remains a key challenge in a broad range of cell types. We designed a robust coselection strategy to perform successive rounds of genetic changes in human cells using CRISPR-Cas nucleases and prime editors. Through coediting, the recovery of cells modified at a target gene of interest is coupled to selection for dominant alleles of the ubiquitous and essential sodium/potassium pump (Na^+/K^+ ATPase). The method improves prime editing efficiency 1.5–10-fold in K562 and HeLa cells, reaching up to 83% of desired alleles in cell populations, for previously optimized prime editing guide RNAs (pegRNAs). Using pegRNAs designed *de novo*, we readily engineered homozygous cell lines with cancer-associated or drug resistant *MTOR* mutations displaying altered mTORC1 signaling. Our approach streamlines the production of cell lines with multiple genetic modifications to create cellular models for biological research and lays the foundation for the development of cell-type specific coselection strategies.

INTRODUCTION

Prime editing (PE) is a genre of genome editing that can be used to install nucleotide substitutions, as well as, short insertions and deletions without requiring donor DNA or double-strand breaks (DSBs)[1–3]. Prime editors are ribonucleoproteins (RNPs) composed of a Cas9 nickase fused to a reverse transcriptase (RT) and a programmable pegRNAs. The pegRNAs are single-guide RNAs (sgRNAs)[4] extended at their 3' ends with two motifs required for initiation of reverse transcription and specification of the genomic changes, namely the primer binding site (PBS) and the RT template[1]. As compared to sgRNAs for CRISPR nucleases and base editors, the design of pegRNAs is more complex since few PBS and RT template combinations are functional in a broad range of cell lines[1]. While the prediction of efficiency of pegRNAs in human cells is making progress[5,6], there remains a need to test many permutations empirically to find optimal reagents.

To date, six types of prime editors are used: PE2, PE3, PE3b, PE4, PE5 and PE5b[1,7]. PE2 relies on an engineered Moloney murine leukemia virus (M-MLV) reverse transcriptase (RT) fused to a SpCas9 nickase (H840A) to introduce small genetic changes templated by the pegRNA. After

54 DNA binding and nicking, PE2 reverse transcribes the intended edit from the pegRNA 3'
55 extension. The resolution of the heteroduplex, by a mechanism that remains incompletely defined,
56 results in the introduction of the intended edit[1–3,7]. The PE3 strategy relies on an additional sgRNA
57 to nick the non-edited strand and direct DNA repair to preferentially incorporate the intended edit
58 which typically results in higher editing efficiency versus PE2[1,3]. However, PE3 can yield a low
59 but detectable rate of indels formation at the target site, decreasing product purity[1,3,8,9]. When
60 permitting, a nicking sgRNA that matches the edited strand can be used to minimize the presence
61 of concurrent nicks, and consequently, indel formation[1]. Denoted as PE3b[1], this strategy is not
62 applicable when no protospacer adjacent motif (PAM) is available near the targeted edit. Transient
63 coexpression of a dominant negative DNA mismatch repair (MMR) protein (MLH1dn) along with
64 PE components further enhances efficiency and lowers editing byproducts[7]. This strategy yielded
65 the PE4 (PE2+MLH1dn), PE5 (PE3+MLH1dn), and PE5b (PE3b+MLH1dn) editors[7]. Thus, the
66 optimal PE strategy to adopt varies according to the context and there is a need to develop methods
67 to consistently improve its success rate.
68
69 To circumvent these limitations several approaches have been implemented including editing with
70 purified ribonucleoprotein complexes (RNPs)[10], mRNA-based delivery[7,11], engineered pegRNAs
71 (epegRNAs)[12], NLS- and codon-optimized prime editors[7,9,13], enrichment with puromycin, and
72 fluorescent reporter-based selection[14–16]. Nevertheless, these improvements are still dependent on
73 extensive pegRNA optimization, absolute activity remains low, and the streamlined production of
74 homozygous cell lines has yet to be achieved[1,12]. Hence, further refinements to these approaches
75 are needed to boost the efficiency of PE in human cells[2,3,7,12].
76
77 We previously reported a robust coselection method for CRISPR nucleases that relies on co-
78 targeting a gene of interest (GOI) and the *ATP1A1* locus to confer dominant cellular resistance to
79 ouabain[17], a plant-derived inhibitor of the ubiquitous and essential Na^+/K^+ ATPase[18,19]. Such an
80 approach derives from the observation that simultaneous targeting of two different loci results in
81 double-editing events that are not statistically independent[17,20–25]. The strategy has proven to be
82 portable to non-homologous end joining (NHEJ), homology directed repair (HDR), and base
83 editing events in near-haploid, diploid and polyploid cells[17,26–32]. To further extend the versatility
84 of this method, we took advantage of the extensive mutagenesis and crystallographic studies that

85 have led to the identification of mutated versions of the enzyme that are resistant to various
86 concentration of ouabain[18,19,33–35]. We engineered these dominant gain-of-function mutations in
87 *ATP1A1* to confer cellular resistance to discrete levels of ouabain, allowing up to three sequential
88 rounds of selection to be performed, by progressively increasing the concentration of the inhibitor
89 at each step. This approach was adapted to enrich PE events in human cells whilst enabling
90 multiple rounds of coselection. Lastly, we demonstrate that *ATP1A1* can be used as a selectable
91 genomic safe harbor[36,37] for targeted integration and long-term expression of transgenes.
92
93 Hence, we propose an easy-to-implement toolkit to select cells engineered via PE without the use
94 of exogenous selection markers that largely bypasses the need for extensive pegRNA optimization.
95 This approach should be compatible with future improvements of the PE technology and should
96 simplify the generation of isogenic panels of human cell lines with multiple genetic modifications.
97

98 # RESULTS

99 **Editing *ATP1A1* to confer discrete levels of resistance to ouabain**

100 The main subunit of the Na^+/K^+-ATPase (a.k.a sodium-potassium pump), encoded by *ATP1A1*, is
101 a 1023 amino acid long protein containing ten transmembrane domains and five extracellular loops
102 which transports Na^+ and K^+ against their electrochemical gradients. It is also the extracellular
103 receptor for cardiac glycosides, a class of drugs that comprises ouabain and digoxin[18,19,38]. A long
104 history of random mutagenesis studies has mapped amino acid residues that alter ouabain
105 sensitivity[34,39]. We previously demonstrated that introducing in-frame deletions at *ATP1A1* exon
106 4, encoding border residues of the first extracellular domain of the Na^+/K^+ ATPase, conferred
107 resistance to ouabain and allowed the co-enrichment of NHEJ events at a second locus of interest[17].
108 We also demonstrated that introducing the Q118R and N129D point mutations at *ATP1A1* exon 4
109 using a single-stranded oligodeoxynucleotide (ssODN) donor and a sgRNA targeting the adjacent
110 intron allowed the enrichment of HDR events at a second locus of interest[17] (**Fig. 1a,b** and
111 **Supplementary Fig. 1**). While point mutations in the first extracellular loop (Q118R/N129D)
112 enabled K562 cells to grow in the presence of ~1000 μM ouabain, cells harboring in-frame
113 deletions only resisted to low doses (<5 μM) (**Fig. 1b**). Since several amino acid substitutions
114 across the protein can confer distinct levels of resistance, we hypothesized that they could be
115 engineered in succession to create variants of the pump that are progressively more resistant. By

116 targeting *ATP1A1* repeatedly, and increasing the dose of ouabain at each step, one could perform
117 sequential rounds of coselection and engineer cell lines with multiple genetic modifications.
118
119 We first tested two mutations (L800K and T804N) located in the third extracellular loop and
120 known to confer an intermediate level of resistance as compared to Q118R and N129D[34,35,40,41].
121 We designed a sgRNA to cleave within *ATP1A1* intron 17 (hereafter named G7) in the vicinity of
122 T804 and used a single-stranded oligodeoxynucleotide (ssODN) to introduce either L800K or
123 T804N (**Supplementary Fig. 1**). Cleaving within the intron allows for seamless induction of
124 recombination within the juxtaposed exon and mitigates the negative impact caused by on-target
125 NHEJ-based mutagenesis of this essential gene[17]. K562 cells were transfected with sgRNA G7
126 along with ssODNs, and growth was monitored after the addition of a low dose of ouabain (0.5
127 μM) which is sufficient to kill all non-edited cells within 48 hours[17]. Only cells bearing the T804N
128 mutation survived selection and titration of ouabain revealed that growth remained robust up to 10
129 μM ouabain (**Fig. 1b**). In addition, as observed when DSBs are induced within *ATP1A1* exon 4[17],
130 cleavage within exon 17 selects for in-frame deletions changing the extracellular loops of the pump
131 and conferring resistance to low concentrations of ouabain (**Fig. 1b** and **Supplementary Fig. 1**).
132 Thus, dominant gain-of-function mutations can also be generated by editing the third extracellular
133 loop of the Na^+/K^+-ATPase and confer an intermediate level of resistance to the drug.
134
135 **Robust coselection of cells with CRISPR-driven HDR events via *ATP1A1* T804N**
136 We then tested whether cointroduction of *ATP1A1* T804N could be used to perform coselection
137 for HDR events. First, we targeted an EBFP expression cassette to the *AAVS1* safe harbor[36] in
138 K562 cells and selected a homozygous clone to monitor its conversion to EGFP through FACS-
139 based analysis (**Fig. 1c** and **Supplementary Fig. 1**)[42,43]. Co-targeting *ATP1A1* and the EBFP
140 reporter yielded a marked increase in EGFP positive cells upon low dose (0.5 μM) ouabain
141 selection (**Fig. 1c**). Similarly, targeted insertion of the coding sequence for fluorescent proteins to
142 *LMNA* and *NPM1*, resulted in successful tagging in ~50% of the selected cells (**Fig. 1d,e**). These
143 levels of improvement are equivalent to the ones observed for coselections using the *ATP1A1*
144 Q118R/N129D mutations[17], indicating that both types of mutations are interchangeable in this
145 context.
146

147 ***ATP1A1* as a selectable genomic safe harbor**

148 We then tested whether *ATP1A1* could be used as a safe harbor for targeted integration of
149 transgenes via intron nesting[44]. In our design, the outcome of HDR is the co-introduction of an
150 ouabain resistant allele (T804N) and an expression cassette in antisense orientation within intron
151 17 to maintain functionality of both *ATP1A1* and the transgene (**Fig. 2a** and **Supplementary Fig.**
152 **2**). We first targeted an expression cassette for the fluorescent protein mScarlet-I to *ATP1A1* intron
153 17 and recovered up to 99% of K562 cells and 88% of HeLa cells expressing the reporter after
154 ouabain selection (**Supplementary Fig. 2**). Targeted integration of the transgenes was confirmed
155 in both cell lines by PCR-based genotyping with primers binding outside the region of homology
156 (out-out PCRs) (**Supplementary Fig. 2**).

157

158 A similar strategy was taken to create a K562 cell line containing a reporter for mTOR signaling.
159 The mTOR signaling indicator (TOSI)[45] was adapted to build a TOSI-mScarlet-I-NLS (mSc-
160 TOSI) fluorescent reporter targeted to the *ATP1A1* locus (**Fig. 2a**). Targeting efficacy was
161 compared to the well-established *AAVS1* safe harbor[36]. In both cases, we obtained almost pure
162 populations of reporter-expressing cells (**Fig. 2a-d** and **Supplementary Fig. 2**). Active mTORC1
163 signaling results in rapid phosphorylation of the mSc-TOSI phosphodegron by S6K,
164 ubiquitination, and degradation by the proteasome while its inhibition stabilises the reporter (**Fig.**
165 **2e**)[45]. Treatment with rapamycin increased the fluorescence signal confirming the functionality of
166 the reporter construct when expressed from both loci (**Fig. 2f**). In selected cell populations,
167 expression of fluorescent transgenes from the *ATP1A1* locus was slightly less intense but was more
168 homogenous than from *AAVS1* as determined by FACS-based analysis (**Fig. 2** and **Supplementary**
169 **Fig. 2**). These results suggest that *ATP1A1* can be used as a selectable genomic safe harbor for
170 targeted integration of reporter transgenes and that targeting efficacy is high enough to work with
171 pools of selected cells, thereby bypassing the need to isolate single-cell derived clones.

172

173 We then tested whether targeted integration of a transgene at *ATP1A1* intron 17 could be coupled
174 to gene inactivation at a second locus of interest. Using K562 cells stably expressing fluorescent
175 reporter genes, we performed proof-of-concept experiments suggesting that concomitant knockout
176 of a GOI and exogenous expression of its mutant version can be achieved (**Supplementary Fig.**

177 **3**). This strategy should facilitate the creation of isogenic panels of cells expressing mutant
178 versions of a gene in a knockout background.
179
180 **Multiple rounds of coselection with CRISPR nucleases by repeated editing at *ATP1A1***
181 Having established that T804N and Q118R/N129D are functionally equivalent for coselection, but
182 that edited cells resist to different concentrations of ouabain, we tested if these mutations could be
183 engineered in succession to create variants of the pump that are progressively more resistant. As a
184 starting point, we used a homogenous population of cells expressing mScarlet-I from *ATP1A1*
185 intron 17. This pool was selected with 0.5 μM ouabain via the co-introduction of T804N (see above
186 and **Supplementary Fig. 2**). We then tagged *NPM1* at its N-terminus by targeted insertion of the
187 coding sequence for mNeonGreen (mNG). Following coselection using 100 μM ouabain via
188 Q118R/N129D, 57% of cells expressed the mNG-NPM1 fusion based on FACS analysis. Targeted
189 integration was further confirmed by out-out PCR (**Supplementary Fig. 4**). All cells maintained
190 expression of mScarlet-I demonstrating sustained function over two rounds of selection
191 (**Supplementary Fig. 4**). Similarly, it was possible to target an expression cassette for mNG within
192 *ATP1A1* intron 4 into a cell line already expressing mScarlet-I from *ATP1A1* intron 17. Upon
193 selection with 100 μM ouabain, 93% of cells expressed both transgenes (**Supplementary Fig. 4**).
194 Therefore, this pool of selected cells had two nested and functional expression cassettes within
195 introns of *ATP1A1* as confirmed via out-out PCR (**Supplementary Figs. 2** and **4**). Since NHEJ-
196 mediated editing at *ATP1A1* conferred the lowest level of resistance, performing an initial step of
197 coselection for NHEJ-mediated gene knockout allowed up to three sequential steps of marker-free
198 selection to be performed (**Supplementary Fig. 5**). Taken together, these results demonstrate that
199 *ATP1A1* can be targeted multiple times to perform sequential rounds of marker-free selection by
200 increasing the dose of ouabain at each step. Overall, this efficient and versatile system simplifies
201 the engineering of human cells containing multiple genetic modifications.
202
203 **Robust coselection for prime editing events**
204 Despite continuous improvements in PE technology, there remains a need to develop universal
205 methods to achieve high levels of editing in bulk populations, especially in MMR-proficient
206 cells[1,7]. As observed with CRISPR-nucleases and base editors[17,26] (see also **Supplementary Fig.**
207 **6**), we hypothesized that cells that are proficient at completing prime editing at the *ATP1A1* locus

208 are more likely to harbor a second prime editing event at a GOI. We first designed pegRNAs to
209 install the Q118R and T804N mutations and confirmed that PE3 conferred resistance to ouabain
210 in K562 cells (**Supplementary Fig. 7**). We then constructed tandem U6-driven pegRNA and nick-
211 inducing sgRNA expression vectors to co-target *ATP1A1* and GOIs using a three vectors PE3
212 system (**Fig. 3a**). We selected eight previously optimized pegRNAs[1] targeting four loci to
213 introduce point mutations, insertions, and deletions to test the impact of coselection in K562 and
214 HeLa S3 cells. These MMR-proficient cell lines are known to display lower PE rates, as opposed
215 to HEK293 cells, and have been extensively used as a model system for PE[1,7]. K562 cells were
216 transfected with PE3 elements and expanded in the presence or absence of 0.5 µM ouabain starting
217 at D3 post-transfection until all non-resistant cells were eliminated, which typically takes 10 days.
218 The frequencies of alleles harboring precise modifications markedly increased after coselection
219 for every pegRNA tested, as determined by BEAT[46] and TIDE[47] analysis (**Fig. 3b,c**). Co-targeting
220 with either PE3-T804N or PE3-Q118R yielded very similar improvements in editing rates without
221 exacerbating indels byproducts (**Fig. 3b,c**). Comparable trends were observed in HeLa S3 cells
222 despite slightly lower absolute levels of efficacy with the most active pegRNAs reaching 59%
223 editing, as compared to 83% in K562 cells (**Supplementary Fig. 9**). In HeLa S3, some pegRNAs
224 with undetectable activity prior to selection reached between 26% and 31% upon coselection
225 (**Supplementary Fig. 9**). Overall, coselection systematically and reproducibly increased prime
226 editing yields.
227
228 **Successive rounds of coselection for prime editing in human cells**
229 We tested if cells having undergone a first round of coselection at GOI A with PE3-T804N were
230 competent for a second round of coselection at GOI B with PE3-Q118R (**Fig. 4a**). A pool of K562
231 cells coselected with PE3-T804N at 0.5 µM ouabain and harboring the *RUNX1* +1 ATG insertion
232 was used as starting material. This population had 80% and 73% PE alleles at *RUNX1* and *ATP1A1*
233 T804N, respectively (see **Fig. 3b**). A successful second round of coselection, testing six different
234 pegRNAs (GOI B), was then performed via *ATP1A1* Q118R using 100 µM ouabain (**Fig. 4b**).
235 Similar results were obtained when the entire process was reproduced using a pool of cells with
236 the *EMX1* +1 G to C modification as starting material (**Fig. 4c**). The level of enrichment in these
237 subsequent rounds of PE paralleled the improvements observed in the first rounds of editing,
238 demonstrating that the two steps of co-selection perform equally well and are independent

239 (compare **Figs. 3** and **4)**. Furthermore, editing levels from the first round of coselection remained
240 stable after the second round of coselection, creating cell pools that are highly modified at both
241 GOI A and GOI B (**Fig. 4b,c**). For example, one pool contained 64% and 84% edited alleles at
242 *FANCF* and *RUNX1*, respectively (**Fig. 4b**). Another pool had 78% and 64% editing at *RUNX1*
243 and *EMX1*, respectively (**Fig. 4c**). These data demonstrate that two rounds of PE can be performed
244 sequentially to considerably enrich cells modified at two positions within the genome.
245
246 **Installation of clinically relevant mutations at *MTOR***
247 The serine/threonine kinase mTOR is a master regulator of eukaryotic cell growth and metabolism
248 that integrates environmental cues. Given its central role in maintaining physiological homeostasis,
249 mTOR mutations lead to a diverse range of diseases, including cancers[48–51]. To determine if co-
250 selection could streamline the production of homozygous cell lines for functional studies, we
251 designed pegRNAs to install well-characterized and clinically relevant *MTOR* hyperactivating
252 mutations[49,50,52,53] or rapamycin resistance mutations[54–56]. While the design and screening of
253 several pegRNAs remains a critical aspect of successful PE[1,7,12], we designed and tested only one
254 pegRNA per target based on previously established rules[1,5] for this proof-of-concept experiment.
255 We designed pegRNAs harboring 25 nucleotides (nts) 3' extensions with 12- to 13-nts PBS and
256 PAM or seed mutations within the RT template to install four hyperactivating mutations (L2431P,
257 E2419K, A2020V, I2017T) and two mutations causing resistance to rapamycin (F2108L, S2035T).
258 To monitor the impact of mTOR variants on signaling activity, PE was performed in a K562 cell
259 line containing the mTOR signaling indicator targeted to *ATP1A1* intron 17 (**Figs. 2** and **5a**).
260
261 The mTOR reporter cell line was transfected with the indicated pegRNAs in a PE3 format and
262 cells were treated or not with 100 μM ouabain starting three days post-transfection. At D14,
263 genomic DNA was extracted and the percentage of PE alleles or indels was quantified. In the
264 selected populations, E2419K increased 4 fold (from 21 to 87%), F2108L went up 5 fold (from 12
265 to 58%), and I2017T rose 10 fold (from 4 to 39%) (**Fig. 5b**). While undetectable before selection,
266 coselection allowed the detection of 12%, 9%, and 6% of alleles harboring L2431P, S2035T, and
267 A2020V, respectively (**Fig. 5b**). Indels remained low with (≤ 8%) after coselection with all *MTOR*
268 pegRNAs (**Fig. 5b**). Notably, hyperactive mTOR signalling could be detected in coselected cell
269 pools indicating that the process provides the means to evaluate variant causality in populations of

270 PE edited cells, thus bypassing the need to isolate single-cell derived clones (**Supplementary Fig.**
271 **11**). Similarly, rapamycin resistance conferred by the F2108L mutation could also be observed in
272 the coselected population (**Supplementary Fig. 11**). The entire gene editing process was
273 reproduced in HeLa S3 cells. First, targeted integration of the mSc-TOSI reporter within *ATP1A1*
274 yielded a cell pool with 99% of cells expressing the transgene (**Supplementary Fig. 12**). However,
275 in these cells the difference in fluorescence observed by FACS-based analysis was too minimal
276 between the on and off states (+/- rapamycin) to monitor the impact of PE-induced mutations
277 (**Supplementary Fig. 12**). Nevertheless, PCR-based genotyping revealed that the percentage of
278 alleles harboring the E2419K, F2108L, and I2017T mutations increased 5 fold for E2419K (from
279 17 to 78%), 4 fold for F2108L (from 9 to 39%), and 8 fold for I2017T (from 4% to 30%)
280 (**Supplementary Fig. 12**). The ratio between PE and indels was lower in HeLa S3 cells than in
281 K562s (**Fig. 5b** and **Supplementary Fig. 12**). Larger PE-driven insertions were also observed in
282 gel-based assays in coselected pools of HeLa S3 but not in K562 cells (**Supplementary Fig. 12**
283 and below).
284
285 To test whether coselection can facilitate the isolation of homozygous clones, we isolated and
286 characterized single cell-derived K562 clones with E2419K, F2108L, and I2017T mutations at
287 *MTOR*. At D3 post transfection, cells were either selected in pools or plated in methylcellulose-
288 containing media with 100 µM ouabain to derive clones. This way, PE efficiency can be compared
289 between pools (see **Fig. 5b**) and clones. Genomic DNA was extracted from each clone and the
290 region surrounding the targets were amplified by PCR. Amplicons were analysed on agarose gels
291 and by Sanger sequencing coupled to trace decomposition by BEAT[46] and TIDE[47]
292 (**Supplementary Figs. 13** and **14**). Taking all three mutations together, only 5 clones did not have
293 at least one pegRNA-specified allele out of 88 clones analysed (**Table 1** and **Supplementary Fig.**
294 **14**). Moreover, 35% (31/88) of the clones were homozygous for the desired mutations. Of note,
295 K562s contain three copies of both *MTOR* and *ATP1A1* (**Supplementary Fig. 14**). Biallelic and
296 monoallelic modifications were observed in 24% (21/88) and 34% (30/88) of the clones,
297 respectively (**Table 1** and **Supplementary Fig. 14**). A wide range of relatively short PE-driven
298 indels were also observed in the clones, including tandem duplications and deletions of sequences
299 found between the two nicks[7,10] (**Supplementary Fig. 13**). This spectrum of byproducts is
300 dissimilar to the ~1-5bp indels typically observed with Cas9 nucleases[57]. Large (> 50 bp) PE-

301 mediated insertions and a few large deletions were observed via gel-based assays (**Supplementary**
302 **Fig. 14**). In fact, most clones (54/57) that were not homozygous for the specified *MTOR* mutations
303 contained undesired indel byproducts (**Table 1** and **Supplementary Fig. 14**). These observations
304 contrast with the relatively low levels of indels detected in cell populations with these pegRNAs
305 (**Fig. 5b**). This suggests that PCR bias in bulk population of cells may lead to an
306 underrepresentation of larger insertions products driven by PE3. Overall, the many genotypes
307 observed at the clone level indicate that polyclonal populations are created during coselection.
308
309 The functional impact of PE-mediated *MTOR* mutations was tested in single cell-derived clones.
310 As expected, degradation of the mSc-TOSI reporter was intensified in homozygous clones
311 harboring E2419K or I2017T hyperactivating mutations (**Fig. 5c**). In contrast, monoallelic
312 E2419K and I2017T clones containing inactivating indels at the remaining alleles displayed
313 crippled mTOR signaling despite growing indistinguishably from all other clones
314 (**Supplementary Fig. 15**). This observation suggests that a single edited allele is not sufficient to
315 hyperactivate mTORC1 signaling in K562 cells, highlighting the importance of carefully
316 genotyping PE-generated clones. Complete rapamycin resistance was also observed in
317 homozygous F2108L clones (**Fig. 5d** and **Supplementary Fig. 15**). First and second generation
318 mTOR inhibitors[56,58] were used to demonstrate the specificity of the F2108L mutations and to
319 show that the reporter still responded to drug treatment after clonal derivation (**Fig. 5d** and
320 **Supplementary Fig. 15**). In addition, all clones used for functional FACS-based assays were
321 homozygous for mSc-TOSI knock-in at *ATP1A1* intron 17 as determined by out-out PCR further
322 indicating that the observed variation in reporter signal were caused by the presence of the desired
323 *MTOR* mutations (**Supplementary Fig. 15**). Note that the wild-type (WT) *MTOR* controls used in
324 these FACS-based assays contained the *ATP1A1* Q118R mutation and were selected with ouabain
325 just like the test samples to mitigate any potential impact of the coselection process itself on the
326 readout of the experiments[59]. Taken together, these data indicate that homozygous clones can be
327 readily isolated via marker-free coselection to characterize pathogenic mutations even when low
328 levels of PE are observed in the starting population.
329
330
331

332 **DISCUSSION**

333 The efficiency of PE fluctuates markedly according to the particular edit, target loci, and cell type[1–
334 3,7]. Despite recent key improvements, it still requires substantial level of optimization to use the
335 technology[7] successfully. In this work, we describe a marker-free coselection strategy that
336 substantially and stably improved the outcome of PE for every pegRNAs tested. The extent of
337 enrichment varies with different pegRNAs, but the strategy greatly facilitates the enrichment of
338 both cell pools and homozygous clones to study the impact of variants on gene function. Due to
339 the high efficiency of deriving novel cell lines, multiple independent cell lines can be analysed to
340 ensure that any unexpected result is not from a clonal artifact[59]. The use of well-characterized
341 dominant gain-of-function mutations[34,35,60,61] in *ATP1A1* introduces minimal modifications to the
342 human genome without detectible effect on cell fitness. For functional studies, any potential impact
343 of the modified sodium-potassium pump on the pathway under study can be easily controlled for
344 using a selected control cell line containing only the *ATP1A1* mutations. Typically, the most
345 efficient strategy for the selection of edited cells is targeting endogenous genes as opposed to the
346 use of exogenous markers[17,20,21,62]. Nonetheless, alternative methods have been described to enrich
347 for edited cells, such as puromycin-based selection strategy and the use of surrogate reporters[14,16].
348 Selecting cells that express all PE components with a selection marker is not sufficient for robust
349 enrichment, while FACS-based cell sorting using exogenous gene markers could be prohibitive
350 for some cell types due to cellular stress[14,16].
351
352 An improvement made to our previously described strategy[17] is the option to perform successive
353 rounds of coselection to install multiple genetic modifications sequentially to derive cell lines.
354 Multiple edits can be engineered at the pool level followed by isolation of clones of interest or new
355 modifications can be added to a previously characterized clone enabling the rapid creation of
356 isogenic cell lines. As the method is portable to CRISPR nucleases, base editors, and prime editors,
357 different types of genomic changes can be implemented. Potential applications include (*i*) gene
358 complementation with variants coupled to endogenous knock out, (*ii*) epitope tagging followed by
359 creation of point mutations, and (*iii*) rescue experiments to confirm causality between edit and
360 phenotype. To create heavily modified human cell lines for applications such as synthetic biology,
361 one could couple our approach with orthogonal coselection approaches based on auxotrophy or
362 toxins[20,62]. As coselection is now a proven and established strategy, it appears that other pathways

363 and systems such as MAPK signaling[63], proteasome[64], translation[65], and other tissue-specificities[66]
364 could form the basis of future applications of the methodology.
365
366 Although a more thorough characterisation will be required to fully establish its full potential, it is
367 worth noting that *ATP1A1* can be used as a selectable genomic safe harbor for targeted integration
368 of transgenes via intron nesting[44]. Stable transgene expression was achieved with a near 1:1
369 correspondence between targeted integration and drug resistance, similar to observations made at
370 the *HBEGF* locus[20].
371
372 While the complete mechanism of action of PE remains to be fully elucidated, DNA mismatch
373 repair (MMR) was identified as a genetic determinant of PE outcome. Specifically, MMR inhibits
374 PE and promotes the formation of undesired indel byproducts[7]. In the context of coselection, clonal
375 analysis revealed a high degree of correlation between editing at *ATP1A1* and modification at three
376 different positions within *MTOR*. As such, only one out of 88 selected clones did not display any
377 gene modification (PE or indels) at *MTOR* and only 5 clones did not have at least one pegRNA-
378 specified allele. This clearly indicates that cells proficient at completing one PE3-driven genomic
379 manipulation have an increased probability of completing a second event at a distinct locus.
380 Moreover, approximately a third (31/88) of selected clones were found to be homozygous for the
381 specified mutations at the *MTOR* locus in the triploid K562 cell line. Interestingly, clones triallelic
382 for the I2017T mutation were observed at a frequency of 30% (8/27) even though PE levels in the
383 pool of selected cells only reached 39%. Thus, when active in a cell, PE is prone to edit more than
384 one allele of its target gene. Taken together, our data suggest that only a fraction of cells in an
385 asynchronous population are competent for PE. Although this observation warrants further
386 investigation, a detailed mechanistic understanding of the PE reaction may help to explain these
387 results. A confounding factor in this analysis may stem from *MTOR*'s essentiality, but we did not
388 observe any growth delay in either pools of cells or when clones developed into colonies in
389 methylcellulose for the various genotypes.
390
391 We selected the PE3 strategy to initiate coselection because it is more active than PE2 in human
392 cells[1,7]. This reduced the time required to obtain a fully resistant population of cells. However, PE3
393 comes at the expense of product purity and is linked to the formation of indels[1,7,10]. Genotyping of

394 single cell-derived clones allowed us to better describe the different types of PE3 byproducts. Our
395 PE3 designs for *MTOR* are all configured with PAMs facing outwards with respect to each other
396 (PAM-out). When combined with the H840A SpCas9 nickase (inactivated HNH domain) it creates
397 DSBs with 3' ssDNA protruding ends ranging from 38 to 50 bases (**Supplementary Fig. 13**). As
398 such, the types of undesirable DNA lesions observed are reminiscent to the repair outcomes
399 occurring when a paired nickase strategy[67] is used to create DSBs with 3' overhangs[57,68]. First, the
400 major repair byproducts are direct repeats of the sequences found within the overhangs[57,68]
401 (**Supplementary Fig. 13**). Mechanistically, fill-in synthesis of the 3' protruding ends by Polα-
402 primase can account for these tandem duplications in a pathway that requires 53BP1[69–71]. Notably,
403 a CRISPRi screen revealed that *TP53BP1* knockdown drastically reduces the frequency of tandem
404 duplications during PE3 (PAM-out)[7] further suggesting that editing byproducts are linked to the
405 DSB repair response resulting from presence of concomitant nicks. Secondly, frequent large
406 insertions were clearly observed in clones via-gel based assays and missed by sequencing bulk
407 populations of prime edited cells (**Supplementary Fig. 14**). To our knowledge, these events have
408 not been reported before and may be composed of multiple repeated sequences formed by
409 consecutive rounds of repair and nicking since the target sites are still present in the tandem
410 duplications[68] (**Supplementary Fig. 13**). Finally, deletions occurring in between the two nicks are
411 larger than normally observed when using WT SpCas9[57] (**Supplementary Fig. 13**).
412
413 Taken together, these data suggest that a competition between PE3 and NHEJ determines the
414 overall efficiency of prime editing. Delaying rapid and predominant NHEJ-mediated repair may
415 improve PE3 yields and purity. DNA end protection mediated by 53BP1[70,72] could modulate PE3
416 outcome as 53BP1-deficient cells have delayed repaired kinetics that can lead to a switch in the
417 choice of repair pathway[73]. Further supporting this view, *TP53BP1* knockdown not only markedly
418 decreases the formation of tandem duplication and deletions but increases the levels of intended
419 edits when PE3 is used in a PAM-out mode[7]. *TP53BP1* knockdown also reduces deletions in the
420 PE3 PAM-in form[7]. This warrant testing of i53 (inhibitor of 53BP1), a genetically encoded
421 inhibitor of 53BP1[74] to enhance PE3, further delineate its mechanism of action, and compare its
422 outcome to PE5. The impact of modulating NHEJ or MMR on genome integrity remains to be
423 fully explored.
424

425 Taken as a whole, the various strategies presented here should further streamline the incorporation
426 of marker-free genetic changes in human cells while being compatible with future improvements
427 in PE technology.
428

429 # METHODS

430 **Cell culture and transfection**

431 K562 cells were obtained from the ATCC (CCL-243) and maintained at 37 °C under 5% CO_2 in
432 RPMI medium supplemented with 10% FBS, penicillin–streptomycin, and GlutaMAX. HeLa S3
433 and U2OS cells were obtained from the ATCC (CCL-2.2 and HTB-96) and maintained at 37 °C
434 under 5% CO_2 in DMEM medium supplemented with 10% FBS, penicillin–streptomycin, and
435 GlutaMAX. Cells were routinely tested for the absence of mycoplasma contamination. Ouabain
436 octahydrate (Sigma) was dissolved at 50 mg/ml in hot water, working dilutions were prepared in
437 water and stored at -20ºC. Rapamycin (Cayman Chemicals) was dissolved at 10 mg/ml in DMSO,
438 working dilutions were prepared in water and stored at -20ºC. AZD8055 (STEMCELL
439 Technologies) was dissolved at 10 mM in DMSO, working dilutions were prepared in water and
440 stored at -20ºC. DMSO alone was diluted in water and used as vehicle control. K562 cells ($2x10^5$
441 cells/transfection) were transfected with an Amaxa 4D-nucleofector™ (Lonza) using the SF
442 nucleofection kit (program FF-120) per manufacturer's recommendations. HeLa S3 cells ($2x10^5$
443 cells/transfection) were transfected using the SE nucleofection kit (Standard HeLa program CN-
444 114 and High efficiency HeLa S3 program DS-150). U2OS cells ($4x10^5$ cells/transfection) were
445 transfected using the SE nucleofection kit (program DN-100). Amounts of DNA used for each
446 experiment can be found in the **Supplementary material** section.
447

448 Cells were treated with the indicated concentrations of ouabain starting 3 days post-nucleofection
449 until all non-resistant cells were eliminated. Typical coselection for prime editing requires 10-14
450 days and 14-21 days for K562 and HeLa S3 cells, respectively. Timing can vary according to initial
451 modification rates at *ATP1A1* and we recommend using the High efficiency HeLa S3 program
452 (DS-150) for HeLa S3 cells. Simultaneous coselection and cloning was performed in
453 methylcellulose-based semi-solid RPMI medium supplemented with 100 µM ouabain for 10 days.
454 To establish the K562 cell line constitutively expressing EBFP and EGFP from the *AAVS1* safe-
455 harbor, cloning was performed in methylcellulose-based semi-solid RPMI medium supplemented

456 with 0.5 µg/ml puromycin for 10 days as previously described[75]. Clones were picked and expanded
457 in 96 wells for 3 days and transferred to 24-well plates for another 3 days before genomic DNA
458 extractions. Clones of interest were then cultured in 6-well plates prior to FACS analysis.
459
460 **Genome editing vectors and reagents**
461 Adenine base editing (ABE) and prime editing (PE) experiments were performed with
462 pCMV_ABEmax[76] (Addgene 112095), ABE8e[77] (Addgene 138489), ABE8e (TadA-8e V106W)[77]
463 (Addgene 138495), pCMV-PE2[1] (Addgene 132775), and pU6-pegRNA-GG-acceptor[1] (Addgene
464 132777). These vectors were gifts from David R. Liu. U6-pegRNA cassette expressing the
465 *ATP1A1*-Q118R and T804N cassettes were cloned upstream of the U6-RFP-acceptor cassette to
466 create *ATP1A1*_G4_Q118R_Dual_pegRNA (Addgene 173199) and *ATP1A1*_G6_T804N
467 _Dual_pegRNA (Addgene 173200). For coselection, pegRNAs targeting GOI were cloned in the
468 dual pegRNA vectors using the same protocol[1]. For PE3 nick gRNAs, gRNAs were cloned into an
469 in-house pUC19-U6-BbsI-sgRNA vector. The U6-*ATP1A1* nick gRNA cassettes were cloned
470 upstream of the U6-BbsI-sgRNA cassette to create *ATP1A1*_G3_Dual_sgRNA (Addgene 173202)
471 and *ATP1A1*_G8 _Dual_sgRNA (Addgene 178104). For PE3 coselection, nick gRNAs targeting
472 the genes of interest were cloned into the BbsI sites of the dual nick gRNA vectors. The U6-
473 *ATP1A1* gRNA (G2) cassette was also cloned upstream of the U6-BbsI-sgRNA cassette to create
474 *ATP1A1*_G2_Dual_sgRNA (Addgene 173201) for ABE coselections. When required, DNA
475 sequences for the guides were modified at position 1 to encode a G, owing to the transcription
476 requirement of the human U6 promoter. All sgRNA, pegRNA, and ssODN sequences used during
477 this study are provided in the **Supplementary material** section.
478
479 For nuclease-based coselections, gRNA sequences were cloned into eSpCas9(1.1)_No_FLAG
480 (Addgene 79877)[75], eSpCas9(1.1)_No_FLAG_*ATP1A1*_G3_Dual_sgRNA1[17] (Addgene 86613)
481 or pX330-U6-Chimeric_BB-CBh-hSpCas9[78] (Addgene 42230), a gift from Feng Zhang. Plasmid
482 donor sequences used for *ATP1A1* gene knock-in were cloned by restriction cloning in a pUC19
483 backbone. All plasmid donor sequences contained short homology arms (< 1 kb) and they were
484 modified to prevent Cas9 cleavage. To repurpose the mTORC1 signaling reporter mVenus-TOSI
485 previously developed for mouse[45], the N-terminal residues (1-82) of the human *PDCD4* gene were
486 codon optimized using the GenSmart™ codon optimization tool, synthesized as a gBlocks™, and

487 cloned into ATP1A1_T804N_hPGK1_mScarlet-I_Donor (Addgene 173207) upstream of the
488 mScarlet-I-NLS cassette using AflII and NcoI. For puromycin selection, the TOSI_mScarlet-I-
489 NLS cassette was transferred to *AAVS1*_Puro_PGK1_3×FLAG_Twin_Strep[75] (Addgene plasmid
490 68375). Desalted ssODNs (see **Supplementary material**) were synthesized as ultramers (IDT) at
491 a 4 nmol scale. A series of vectors described in this work (see **Supplementary material)** have
492 been deposited to Addgene.
493
494 **Flow cytometry**
495 The percentage of fluorescent cells was quantified using a BD LSRII flow cytometer and $1x10^5$
496 cells were analyzed for each condition. When HDR donor plasmids harboring a human *PGK1*
497 promoter were used to target fluorescent gene cassettes to the *ATP1A1* locus, cells were cultured
498 for 21 days to eliminate residual expression from non-integrated reporter cassettes. For mTORC1
499 signaling assays, cells were treated with the indicated concentration of rapamycin or AZD8055 for
500 24 hours before analysis. Flow cytometric data visualization and analysis was performed using
501 FlowJo software (Tree Star).
502
503 **Genotyping**
504 Genomic DNA was extracted with QuickExtract DNA extraction solution (EpiCentre) following
505 manufacturer's recommendations. Primers used in this study and the PCR product sizes are
506 provided in the **Supplementary material** section. All PCR amplifications were performed with
507 30 cycles of amplification. Sanger sequencing was performed on PCR amplicons to quantify the
508 percentage of edited alleles using BEAT, TIDE, and TIDER[16,17,21]. Phusion and Q5 high-fidelity
509 DNA polymerases were used for PCR amplification. Kapa-HiFi polymerase was used for out-out
510 PCRs. To detect targeted integration, out-out PCRs were performed with primers that bind outside
511 of the homology regions of the donor plasmids. Wild type K562 genomic DNA was used as a
512 negative control for all out-out PCRs.
513
514

515 **REFERENCES**

516 1. Anzalone, A. V. *et al.* Search-and-replace genome editing without double-strand breaks or
517 donor DNA. *Nature* **576**, 149–157 (2019).
518 2. Yan, J., Cirincione, A. & Adamson, B. Prime editing: Precision genome editing by reverse
519 transcription. *Mol. Cell* **77**, 210–212 (2020).
520 3. Anzalone, A. V, Koblan, L. W. & Liu, D. R. Genome editing with CRISPR–Cas
521 nucleases, base editors, transposases and prime editors. *Nat. Biotechnol.* **38**, 824–844
522 (2020).
523 4. Jinek, M. *et al.* A programmable dual-RNA-guided DNA endonuclease in adaptive
524 bacterial immunity. *Science (80-.).* **337**, 816–822 (2012).
525 5. Kim, H. K. *et al.* Predicting the efficiency of prime editing guide RNAs in human cells.
526 *Nat. Biotechnol.* **39**, 198–206 (2021).
527 6. Hsu, J. Y. *et al.* PrimeDesign software for rapid and simplified design of prime editing
528 guide RNAs. *Nat. Commun.* **12**, 1034 (2021).
529 7. Chen, P. J. *et al.* Enhanced prime editing systems by manipulating cellular determinants of
530 editing outcomes. *Cell* **184**, 5635–5652 (2021).
531 8. Jang, H. *et al.* Application of prime editing to the correction of mutations and phenotypes
532 in adult mice with liver and eye diseases. *Nat. Biomed. Eng.* (2021) doi:10.1038/s41551-
533 021-00788-9.
534 9. Liu, P. *et al.* Improved prime editors enable pathogenic allele correction and cancer
535 modelling in adult mice. *Nat. Commun.* **12**, 2121 (2021).
536 10. Petri, K. *et al.* CRISPR prime editing with ribonucleoprotein complexes in zebrafish and
537 primary human cells. *Nat. Biotechnol.* (2021) doi:10.1038/s41587-021-00901-y.
538 11. Sürün, D. *et al.* Efficient generation and correction of mutations in human iPS cells
539 utilizing mRNAs of CRISPR base editors and prime editors. *Genes (Basel)* **11**, 511
540 (2020).
541 12. Nelson, J. W. *et al.* Engineered pegRNAs improve prime editing efficiency. *Nat.*
542 *Biotechnol.* (2021) doi:10.1038/s41587-021-01039-7.
543 13. Park, S. J. *et al.* Targeted mutagenesis in mouse cells and embryos using an enhanced
544 prime editor. *Genome Biol.* **22**, 170 (2021).
545 14. Adikusuma, F. *et al.* Optimized nickase- and nuclease-based prime editing in human and

546 mouse cells. *Nucleic Acids Res.* **49**, 10785–10795 (2021).
547 15. Schene, I. F. *et al.* Prime editing for functional repair in patient-derived disease models.
548 *Nat. Commun.* **11**, 5352 (2020).
549 16. Simon, D. A., Tálas, A., Kulcsár, P. I. & Welker, E. PEAR: a flexible fluorescent reporter
550 for the identification and enrichment of successfully prime edited cells. *BioRxiv*
551 https://doi.org/10.1101/2021.04.26.441486 (2021).
552 17. Agudelo, D. *et al.* Marker-free coselection for CRISPR-driven genome editing in human
553 cells. *Nat. Methods* **14**, 615–620 (2017).
554 18. Laursen, M., Gregersen, J. L., Yatime, L., Nissen, P. & Fedosova, N. U. Structures and
555 characterization of digoxin- and bufalin-bound Na+,K+-ATPase compared with the
556 ouabain-bound complex. *Proc. Natl. Acad. Sci.* **112**, 1755–1760 (2015).
557 19. Ogawa, H., Shinoda, T., Cornelius, F. & Toyoshima, C. Crystal structure of the sodium-
558 potassium pump (Na+,K+-ATPase) with bound potassium and ouabain. *Proc. Natl. Acad.*
559 *Sci.* **106**, 13742–13747 (2009).
560 20. Li, S. *et al.* Universal toxin-based selection for precise genome engineering in human
561 cells. *Nat. Commun.* **12**, 497 (2021).
562 21. Ren, C., Xu, K., Segal, D. J. & Zhang, Z. Strategies for the enrichment and selection of
563 genetically modified cells. *Trends Biotechnol.* **37**, 56–71 (2019).
564 22. Arribere, J. A. *et al.* Efficient marker-free recovery of custom genetic modifications with
565 CRISPR/Cas9 in Caenorhabditis elegans. *Genetics* **198**, 837–846 (2014).
566 23. Kim, H. *et al.* A Co-CRISPR strategy for efficient genome editing in Caenorhabditis
567 elegans. *Genetics* **197**, 1069–1080 (2014).
568 24. Kane, N. S., Vora, M., Varre, K. J. & Padgett, R. W. Efficient screening of CRISPR/Cas9-
569 induced events in Drosophila using a Co-CRISPR strategy. *G3* **7**, 87–93 (2017).
570 25. Tianfang Ge, D., Tipping, C., Brodsky, M. H. & Zamore, P. D. Rapid screening for
571 CRISPR-directed editing of the Drosophila genome using white coconversion. *G3* **6**,
572 3197–3206 (2016).
573 26. Billon, P. *et al.* CRISPR-mediated base editing enables efficient disruption of eukaryotic
574 genes through induction of STOP codons. *Mol. Cell* **67**, 1068-1079.e4 (2017).
575 27. Eaton, J. D., Francis, L., Davidson, L. & West, S. A unified allosteric/torpedo mechanism
576 for transcriptional termination on human protein-coding genes. *Genes Dev.* **34**, 132–145

577 (2020).
578 28. Lamaa, A. *et al.* Integrated analysis of H2A.Z isoforms function reveals a complex
579 interplay in gene regulation. *Elife* **9**, 1–27 (2020).
580 29. Cerezo, E. L. *et al.* RIOSK2 phosphorylation by RSK promotes synthesis of the human
581 small ribosomal subunit. *PLoS Genet.* **17**, e1009583 (2021).
582 30. Hellmuth, S. & Stemmann, O. Separase-triggered apoptosis enforces minimal length of
583 mitosis. *Nature* **580**, 542–547 (2020).
584 31. Maurissen, T. L. & Woltjen, K. Synergistic gene editing in human iPS cells via cell cycle
585 and DNA repair modulation. *Nat. Commun.* **11**, (2020).
586 32. Robinson, K. S. *et al.* Enteroviral 3C protease activates the human NLRP1 inflammasome
587 in airway epithelia. *Science* **370**, 1182 (2020).
588 33. Price, E. M., Rice, D. A. & Lingrel, J. B. Structure-function studies of Na,K-ATPase: site-
589 directed mutagenesis of the border residues from the H1-H2 extracellular domain of the
590 alpha subunit. *J. Biol. Chem.* **265**, 6638–6641 (1990).
591 34. Croyle, M. L., Woo, A. L. & Lingrel, J. B. Extensive random mutagenesis analysis of the
592 Na+/K+-ATPase α subunit identifies known and previously unidentified amino acid
593 residues that alter ouabain sensitivity: Implications for ouabain binding. *Eur. J. Biochem.*
594 **248**, 488–495 (1997).
595 35. Burns, E. L. & Price, E. M. Random mutagenesis of the sheep Na,K-ATPase α-1 subunit
596 generates a novel T797N mutation that results in a ouabain-resistant enzyme. *J. Biol.*
597 *Chem.* **268**, 25632–25635 (1993).
598 36. Dekelver, R., Choi, V. & Moehle, E. Functional genomics, proteomics, and regulatory
599 DNA analysis in isogenic settings using zinc finger nuclease-driven transgenesis into a
600 safe harbor locus in the human genome. *Genome Res.* **20**, 1133–1142 (2010).
601 37. Irion, S. *et al.* Identification and targeting of the ROSA26 locus in human embryonic stem
602 cells. *Nat. Biotechnol.* **25**, 1477–1482 (2007).
603 38. Laursen, M., Yatime, L., Nissen, P. & Fedosova, N. U. Crystal structure of the high-
604 affinity Na+,K+-ATPase-ouabain complex with Mg2+ bound in the cation binding site.
605 *Proc. Natl. Acad. Sci.* **110**, 10958–10963 (2013).
606 39. Aardema, M. L., Zhen, Y., Schumer, M., Andolfatto, P. & Medina, E. M. Parallel
607 Molecular Evolution in an Herbivore Community. *Science* **337**, 1634–1637 (2012).

608 40. Burns, E. L., Nicholas, R. A. & Price, E. M. Random mutagenesis of the sheep Na,K-
609 ATPase α1 subunit generating the ouabain-resistant mutant L793P. *J. Biol. Chem.* **271**,
610 15879–15883 (1996).
611 41. Qiu, L. Y., Koenderink, J. B., Swarts, H. G. P., Willems, P. H. G. M. & De Pont, J. J. H.
612 H. M. Phe783, Thr797, and Asp804 in transmembrane hairpin M5-M6 of Na+,K+-
613 ATPase play a key role in ouabain binding. *J. Biol. Chem.* **278**, 47240–47244 (2003).
614 42. Richardson, C. D., Ray, G. J., DeWitt, M. A., Curie, G. L. & Corn, J. E. Enhancing
615 homology-directed genome editing by catalytically active and inactive CRISPR-Cas9
616 using asymmetric donor DNA. *Nat. Biotechnol.* **34**, 339–344 (2016).
617 43. Glaser, A., McColl, B. & Vadolas, J. GFP to BFP conversion: A versatile assay for the
618 quantification of CRISPR/Cas9-mediated genome editing. *Mol. Ther. - Nucleic Acids* **5**,
619 e334 (2016).
620 44. Wright, B. W., Molloy, M. P. & Jaschke, P. R. Overlapping genes in natural and
621 engineered genomes. *Nat. Rev. Genet.* (2021) doi:10.1038/s41576-021-00417-w.
622 45. Oki, T. *et al.* Imaging dynamic mTORC1 pathway activity in vivo reveals marked shifts
623 that support time-specific inhibitor therapy in AML. *Nat. Commun.* **12**, 245 (2021).
624 46. Xu, L., Liu, Y. & Han, R. BEAT: A Python program to quantify base editing from Sanger
625 sequencing. *Cris. J.* **2**, 223–229 (2019).
626 47. Brinkman, E. K. *et al.* Easy quantification of template-directed CRISPR/Cas9 editing.
627 *Nucleic Acids Res.* **46**, e58 (2018).
628 48. Murugan, A. K., Alzahrani, A. & Xing, M. Mutations in critical domains confer the
629 human mTOR gene strong tumorigenicity. *J. Biol. Chem.* **288**, 6511–6521 (2013).
630 49. Wagle, N. *et al.* Activating mTOR mutations in a patient with an extraordinary response
631 on a phase I trial of everolimus and pazopanib. *Cancer Discov.* **4**, 546–553 (2014).
632 50. Endesfelder, D. *et al.* Intratumor heterogeneity and branched evolution revealed by
633 multiregion sequencing. *N. Engl. J. Med.* **366**, 883–892 (2012).
634 51. Grabiner, B. C. *et al.* A diverse array of cancer-associated MTOR mutations are
635 hyperactivating and can predict rapamycin sensitivity. *Cancer Discov.* **4**, 554–563 (2014).
636 52. Ohne, Y. *et al.* Isolation of hyperactive mutants of mammalian target of rapamycin. *J.*
637 *Biol. Chem.* **283**, 31861–31870 (2008).
638 53. Urano, J. *et al.* Point mutations in TOR confer Rheb-independent growth in fission yeast

639 and nutrient-independent mammalian TOR signaling in mammalian cells. *Proc. Natl.*
640 *Acad. Sci.* **104**, 3514–3519 (2007).
641 54. Brown, E. J. *et al.* Control of p70 S6 kinase by kinase activity of FRAP in vivo. *Nature*
642 **377**, 441–446 (1995).
643 55. Wagle, N. *et al.* Response and acquired resistance to everolimus in anaplastic thyroid
644 cancer. *N. Engl. J. Med.* **371**, 1426–1433 (2014).
645 56. Rodrik-Outmezguine, V. S. *et al.* Overcoming mTOR resistance mutations with a new-
646 generation mTOR inhibitor. *Nature* **534**, 272–276 (2016).
647 57. Bothmer, A. *et al.* Characterization of the interplay between DNA repair and
648 CRISPR/Cas9-induced DNA lesions at an endogenous locus. *Nat. Commun.* **8**, 13905
649 (2017).
650 58. Chresta, C. M. *et al.* AZD8055 is a potent, selective, and orally bioavailable ATP-
651 competitive mammalian target of rapamycin kinase inhibitor with in vitro and in vivo
652 antitumor activity. *Cancer Res.* **70**, 288–298 (2010).
653 59. Giuliano, C. J., Lin, A., Girish, V. & Sheltzer, J. M. Generating single cell-derived
654 knockout clones in mammalian cells with CRISPR/Cas9. *Curr. Protoc. Mol. Biol.* **128**,
655 e100 (2019).
656 60. Karageorgi, M. *et al.* Genome editing retraces the evolution of toxin resistance in the
657 monarch butterfly. *Nature* **574**, 409–412 (2019).
658 61. Ujvari, B. *et al.* Widespread convergence in toxin resistance by predictable molecular
659 evolution. *Proc. Natl. Acad. Sci.* **112**, 11911–11916 (2015).
660 62. Wiebking, V. *et al.* Metabolic engineering generates a transgene-free safety for cell
661 therapy. *Nat. Biotechnol.* **38**, 1441–1450 (2020).
662 63. Donovan, K. F. *et al.* Creation of novel protein variants with CRISPR/Cas9-mediated
663 mutagenesis: Turning a screening by-product into a discovery tool. *PLoS One* **12**,
664 e0170445 (2017).
665 64. Hess, G. T. *et al.* Directed evolution using dCas9-targeted somatic hypermutation in
666 mammalian cells. *Nat. Methods* **13**, 1036–1042 (2016).
667 65. Chu, J. *et al.* CRISPR-mediated drug-target validation reveals selective pharmacological
668 inhibition of the RNA helicase, eIF4A. *Cell Rep.* **15**, 2340–2347 (2016).
669 66. Nagree, M. S., López-Vásquez, L., Medin Murtaza S Nagree, J. A., Medin, J. A. & To, C.

670 Towards in vivo amplification: Overcoming hurdles in the use of hematopoietic stem cells
671 in transplantation and gene therapy. *World J. Stem Cells* **7**, 1233–1250 (2015).
672 67. Ran, F. A. *et al.* Double nicking by RNA-guided CRISPR Cas9 for enhanced genome
673 editing specificity. *Cell* **154**, 1380–1389 (2013).
674 68. Schimmel, J., Kool, H., van Schendel, R. & Tijsterman, M. Mutational signatures of non-
675 homologous and polymerase theta-mediated end-joining in embryonic stem cells. *EMBO*
676 *J.* **36**, 3634–3649 (2017).
677 69. Schimmel, J., Muñoz-Subirana, N., Kool, H., van Schendel, R. & Tijsterman, M. Small
678 tandem DNA duplications result from CST-guided Pol α-primase action at DNA break
679 termini. *Nat. Commun.* **12**, 4843 (2021).
680 70. Mirman, Z. & de Lange, T. 53BP1: a DSB escort. *Genes Dev.* **34**, 7–23 (2020).
681 71. Paiano, J. *et al.* Role of 53BP1 in end protection and DNA synthesis at DNA breaks.
682 *Genes Dev.* **35**, 1356–1368 (2021).
683 72. Zhao, B., Rothenberg, E., Ramsden, D. A. & Lieber, M. R. The molecular basis and
684 disease relevance of non-homologous DNA end joining. *Nat. Rev. Mol. Cell Biol.* **21**,
685 765–781 (2020).
686 73. Yamane, A. *et al.* RPA accumulation during class switch recombination represents 5'-3'
687 DNA-end resection during the S-G2/M phase of the cell cycle. *Cell Rep.* **3**, 138–147
688 (2013).
689 74. Canny, M. D. *et al.* Inhibition of 53BP1 favors homology-dependent DNA repair and
690 increases CRISPR-Cas9 genome-editing efficiency. *Nat. Biotechnol.* **36**, 95–102 (2018).
691 75. Dalvai, M. *et al.* A scalable genome-editing-based approach for mapping multiprotein
692 complexes in human cells. *Cell Rep.* **13**, 621–633 (2015).
693 76. Koblan, L. W. *et al.* Improving cytidine and adenine base editors by expression
694 optimization and ancestral reconstruction. *Nat. Biotechnol.* **36**, 843–848 (2018).
695 77. Richter, M. F. *et al.* Phage-assisted evolution of an adenine base editor with improved Cas
696 domain compatibility and activity. *Nat. Biotechnol.* **38**, 883–891 (2020).
697 78. Cong, L. *et al.* Multiplex genome engineering using CRISPR/Cas systems. *Science* **339**,
698 819–823 (2013).
699
700

ACKNOWLEDGEMENTS

This study was supported by a grant from the Natural Sciences and Engineering Research Council of Canada (RGPIN-2014-059680). S.L. holds a Frederick Banting and Charles Best Canada graduate scholarship from CIHR. A.D. holds a doctoral training award from the Fonds de recherche du Québec en Santé (FRQS). D.A. holds a Vanier Canada graduate scholarship from CIHR. Salary support was provided by the Fonds de la Recherche du Québec-Santé (FRQS) to Y.D. We thank the staff at the flow cytometry core facility of the CHU de Quebec Research Center for their training and assistance.

AUTHOR'S CONTRIBUTIONS

Conceptualization, S.L. and Y.D.; methodology, S.L., D.M., J-P.F., C.G., A.D., A.L., E.B., D.A., and Y.D.; investigation, S.L., D.M., J-P.F., C.G., A.D., A.L., E.B., D.A., and Y.D.; writing original draft, S.L.; writing, review and editing, S.L., and Y.D.; supervision, Y.D.; funding acquisition, Y.D. All authors reviewed the manuscript and approved its final version.

COMPETING INTERESTS

The authors declare they have no financial competing interests

Table 1: Distribution of alleles in single cell-derived clones edited at *MTOR* by coselection

MTOR **mutation**	**% of clones with indicated alleles**				
	WT	**WT + Indels**	**Monoallelic PE***	**Biallelic PE***	**Triallelic PE&**
E2419K	0% (0/30)	0% (0/30)	40% (12/30)	33% (10/30)	27% (8/30)
F2108L	0% (0/31)	6% (2/31)	26% (8/31)	19% (6/31)	48% (15/31)
I2017T	4% (1/27)	11% (3/27)	37% (10/27)	19% (5/27)	30% (8/27)
Total	1% (1/88)	6% (5/88)	34% (30/88)	24% (21/88)	35% (31/88)

*Indels are detected on remaining alleles

&Homozygous

a

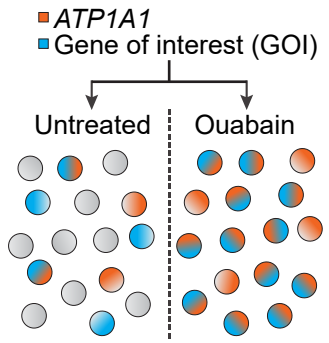

b

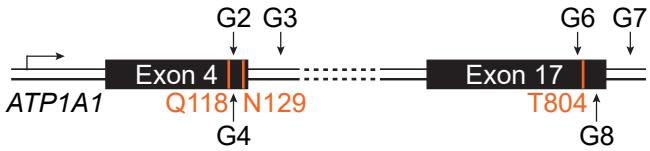

ATP1A1	Mutation(s)	Guide	Ouabain^R
Exon 4	Q118R/N129D	G3	> 1000 μM
Exon 4	N129D	G3	500 μM
Exon 4	Q118R	G3	250 μM
Exon 4	In-frame deletion	G2	≤ 5 μM
Exon 17	T804N	G7	10 μM
Exon 17	In-frame deletion	G6	≤ 5 μM

c

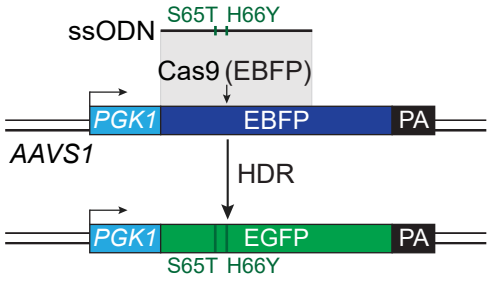

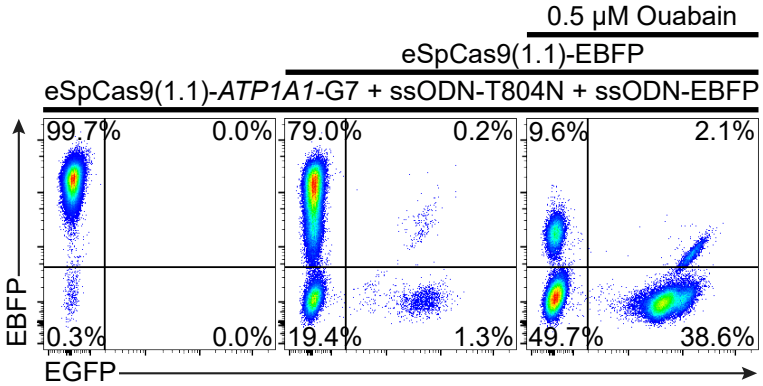

d

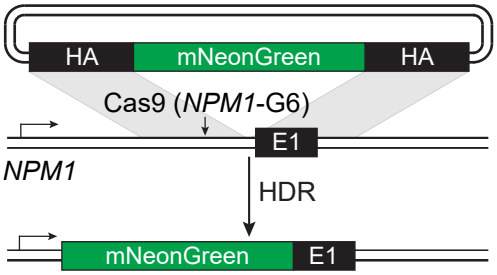

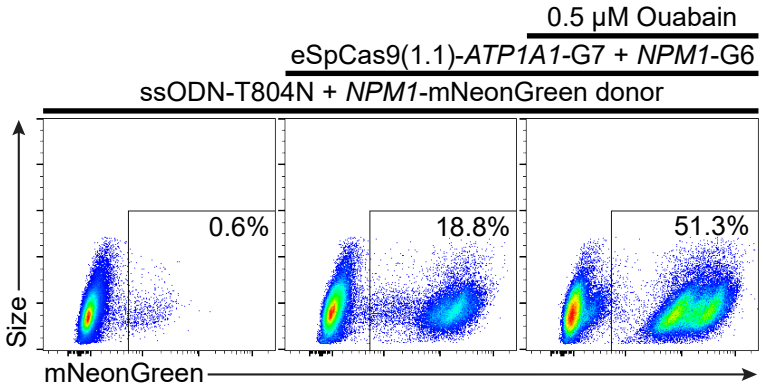

e

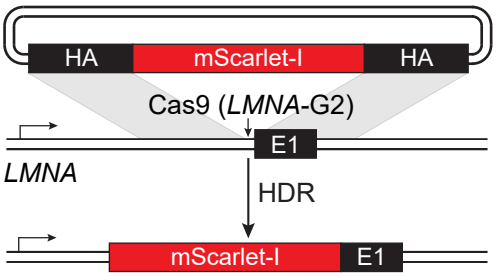

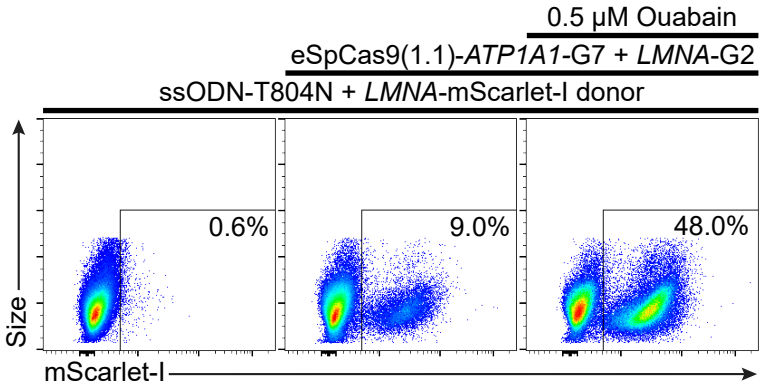

Figure 1. Coselection for HDR-driven events by coediting *ATP1A1* exon 17. (**a**) Schematic for the co-enrichment of CRISPR-driven editing events at a GOI. (**b**) Schematic representation of the *ATP1A1* locus regions targeted by SpCas9. The first and third extracellular loops of the Na^+/K^+ ATPase are encoded by *ATP1A1* exon 4 and 17, respectively. The relative levels of resistance to ouabain conferred by different *ATP1A1* mutations in K562 cells are shown. (**c**) FACS-based quantification of EBFP to EGFP conversion. K562 cells stably expressing EBFP were transfected with nuclease vectors and ssODN donors targeting *ATP1A1* and EBFP. Where indicated, cells were treated with 0.5 μM ouabain starting 3 days post-transfection and expanded until all non-resistant cells were eliminated. (**d**) FACS-based quantification of HDR-driven tagging of *NPM1* with mNeonGreen. K562 cells were transfected with nuclease vectors and donors targeting *ATP1A1* and *NPM1*. Where indicated, cells were treated with 0.5 μM ouabain starting 3 days post-transfection and expanded until all non-resistant cells were eliminated. (**e**) Same as in (**d**) for HDR-driven tagging of *LMNA* with mScarlet-I. *PGK1*, human phosphoglycerate kinase 1 promoter. PA, polyadenylation signal. HA, homology arm. E, exon.

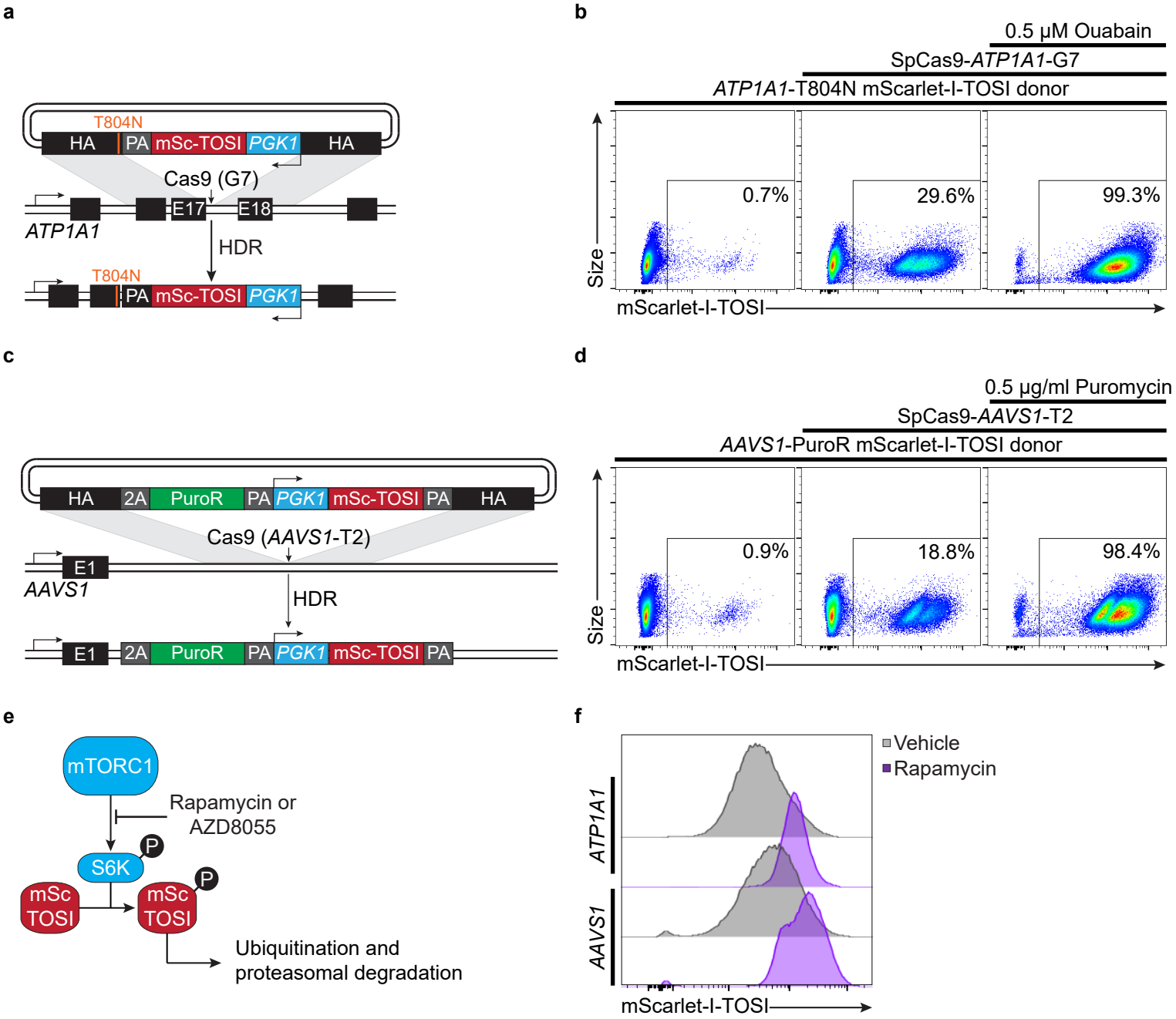
a
T804N
HA
PA
mSc-TOSI
PGK1
HA
Cas9 (G7)
E17
E18
ATP1A1
HDR
T804N
PA
mSc-TOSI
PGK1
b
0.5 μM Ouabain
SpCas9-ATP1A1-G7
ATP1A1-T804N mScarlet-I-TOSI donor
0.7%
29.6%
99.3%
Size
mScarlet-I-TOSI
c
HA
2A
PuroR
PA
PGK1
mSc-TOSI
PA
HA
Cas9 (AAVS1-T2)
E1
AAVS1
HDR
E1
2A
PuroR
PA
PGK1
mSc-TOSI
PA
d
0.5 μg/ml Puromycin
SpCas9-AAVS1-T2
AAVS1-PuroR mScarlet-I-TOSI donor
0.9%
18.8%
98.4%
Size
mScarlet-I-TOSI
e
mTORC1
Rapamycin or
AZD8055
S6K
P
mSc
TOSI
mSc
TOSI
P
Ubiquitination and
proteasomal degradation
f
Vehicle
Rapamycin
ATP1A1
AAVS1
mScarlet-I-TOSI

Figure 2. *ATP1A1* as a selectable genomic safe harbor for targeted integration of transgenes. (**a**) Schematic representation of the targeted integration of mScarlet-I mTOR Signaling Indicator (mSc-TOSI) in antisense orientation within intron 17 of *ATP1A1*. The T804N mutation is introduced via the left homology arm (HA) and transgene expression is driven by the *PGK1* promoter. (**b**) FACS-based quantification of mSc-TOSI knock-in at *ATP1A1* intron 17. K562 cells were transfected with SpCas9 and the donor and treated with or without 0.5 μM ouabain starting 3 days post-transfection until all non-resistant cells were eliminated. (**c**) Schematic representation of mSc-TOSI targeting to the *AAVS1* locus. (**d**) FACS-based quantification of mSc-TOSI knock-in at *AAVS1*. K562 cells were transfected with SpCas9 and a donor targeting *AAVS1* and treated with or without 0.5 μg/ml puromycin starting 3 days post-transfection until all non-resistant cells were eliminated. (**e**) Schematic of mSc-TOSI degradation under mTORC1 signaling. (**f**) mSc-TOSI fluorescence intensity after stable integration at the *ATP1A1* and *AAVS1* loci in presence and absence of rapamycin. Where indicated, cells were treated with 500 nM rapamycin or vehicle control for 24 hours before FACS analysis. *PGK1*, human phosphoglycerate kinase 1 promoter. PA, polyadenylation signal. HA, homology arm. E, exon.

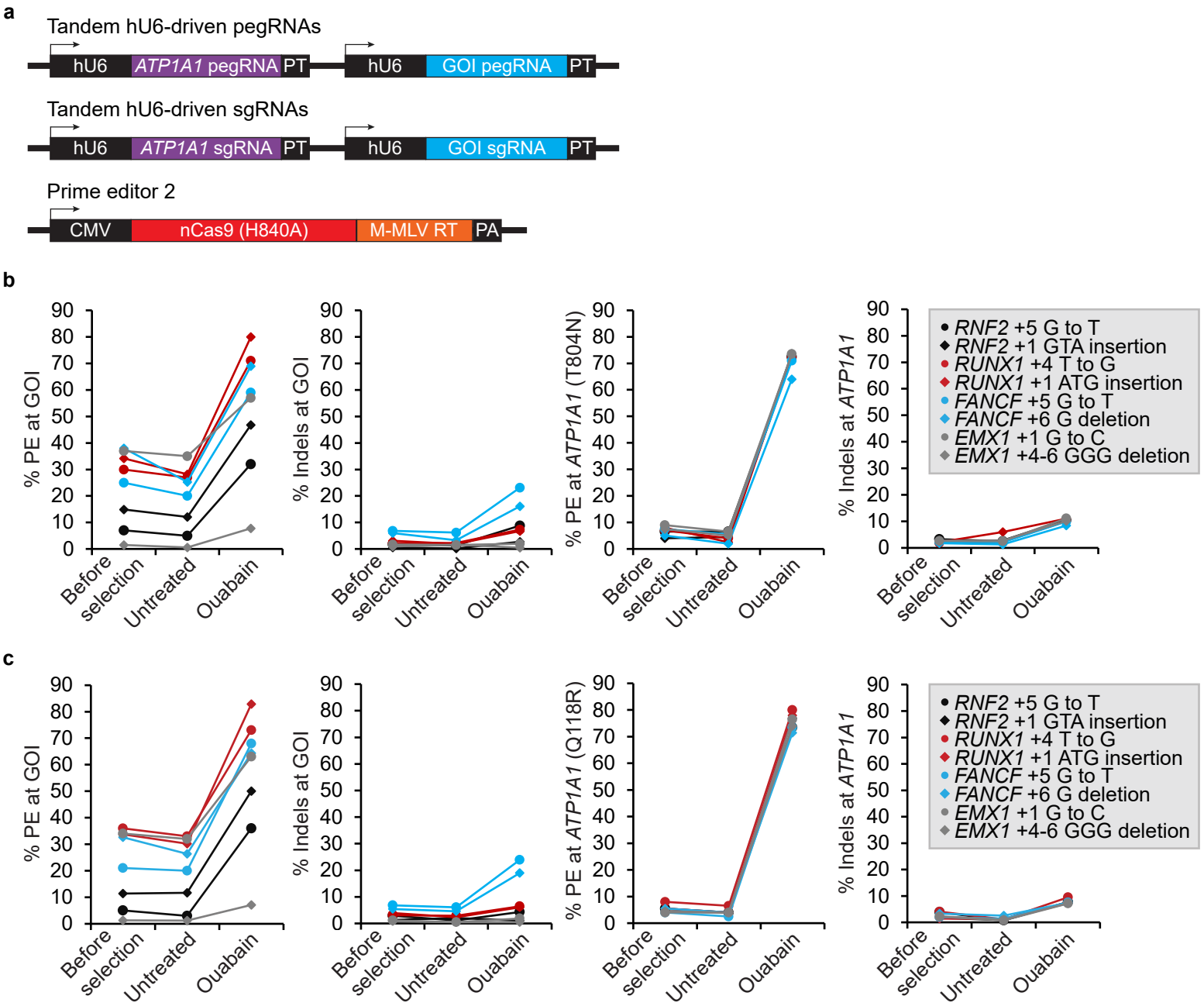
a
Tandem hU6-driven pegRNAs
hU6
ATP1A1 pegRNA
PT
hU6
GOI pegRNA
PT
Tandem hU6-driven sgRNAs
hU6
ATP1A1 sgRNA
PT
hU6
GOI sgRNA
PT
Prime editor 2
CMV
nCas9 (H840A)
M-MLV RT
PA
b
% PE at GOI
% Indels at GOI
% PE at ATP1A1 (T804N)
% Indels at ATP1A1
Before selection
Untreated
Ouabain
RNF2 +5 G to T
RNF2 +1 GTA insertion
RUNX1 +4 T to G
RUNX1 +1 ATG insertion
FANCF +5 G to T
FANCF +6 G deletion
EMX1 +1 G to C
EMX1 +4-6 GGG deletion
c
% PE at GOI
% Indels at GOI
% PE at ATP1A1 (Q118R)
% Indels at ATP1A1
Before selection
Untreated
Ouabain
RNF2 +5 G to T
RNF2 +1 GTA insertion
RUNX1 +4 T to G
RUNX1 +1 ATG insertion
FANCF +5 G to T
FANCF +6 G deletion
EMX1 +1 G to C
EMX1 +4-6 GGG deletion

Figure 3. Robust coselection for prime editing. (**a**) Schematic of the dual and tandem U6-driven pegRNAs and sgRNAs expression vectors along with the PE2 expression vector used to target *ATP1A1* and a GOI. (**b**) PE and indels quantification as determined by BEAT and TIDE analysis from Sanger sequencing. K562 cells were transfected with PE3 vectors targeting *ATP1A1* exon 17 (T804N) and the indicated GOI. Genomic DNA was harvested 3 days post-transfection (before selection) and cells were treated (ouabain) or not (untreated) with 0.5 μM ouabain until all non-resistant cells were eliminated. (**c**) Same as in (**b**) but co-targeting was performed via *ATP1A1* exon 4 (Q118R). These experiments were performed twice and at different times with equivalent results (see also **Supplementary Fig. 8**).

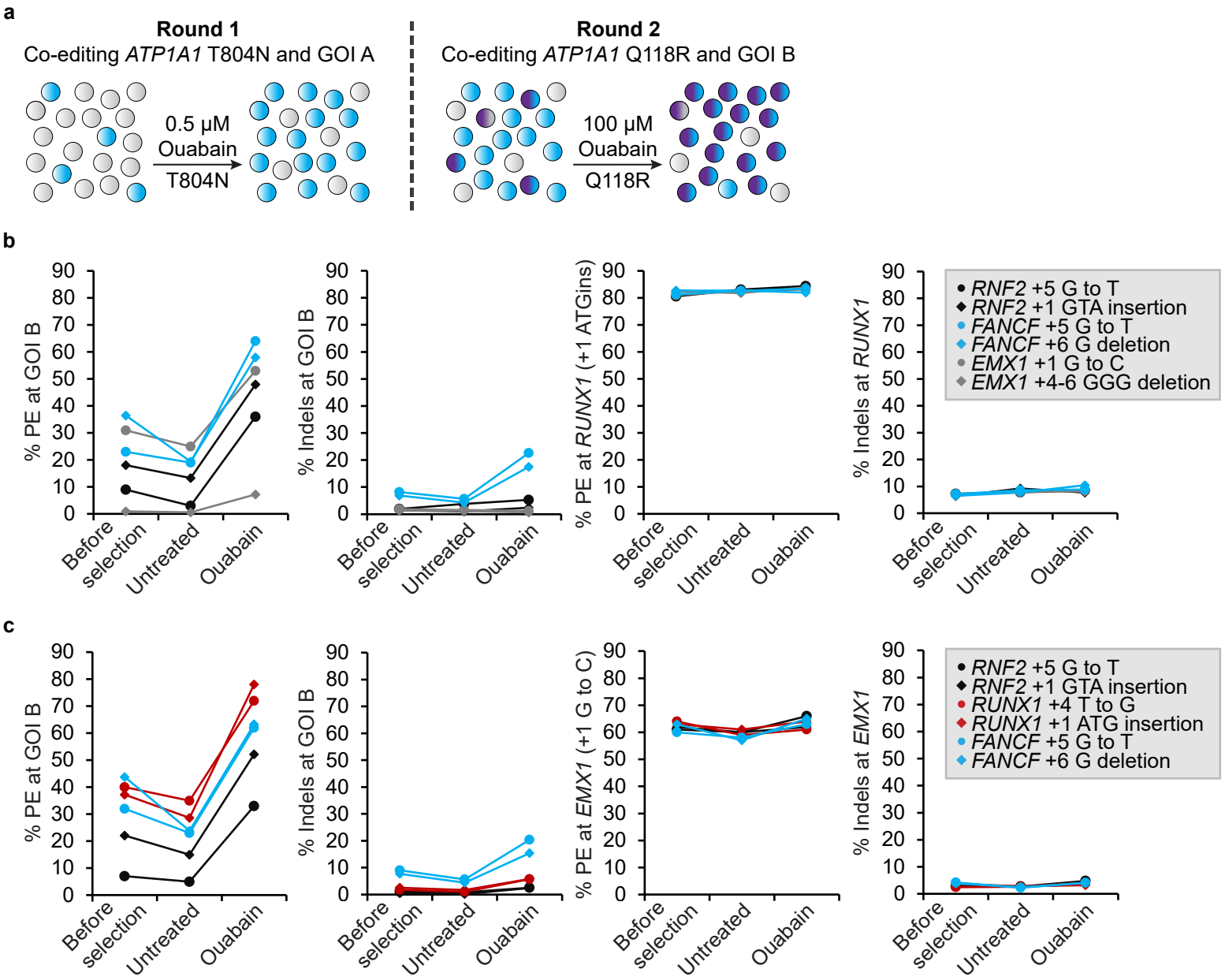
a
Round 1
Co-editing ATP1A1 T804N and GOI A
0.5 μM
Ouabain
T804N
Round 2
Co-editing ATP1A1 Q118R and GOI B
100 μM
Ouabain
Q118R
b
% PE at GOI B
% Indels at GOI B
% PE at RUNX1 (+1 ATGins)
% Indels at RUNX1
Before selection
Untreated
Ouabain
RNF2 +5 G to T
RNF2 +1 GTA insertion
FANCF +5 G to T
FANCF +6 G deletion
EMX1 +1 G to C
EMX1 +4-6 GGG deletion
c
% PE at GOI B
% Indels at GOI B
% PE at EMX1 (+1 G to C)
% Indels at EMX1
RNF2 +5 G to T
RNF2 +1 GTA insertion
RUNX1 +4 T to G
RUNX1 +1 ATG insertion
FANCF +5 G to T
FANCF +6 G deletion

Figure 4. Robust coselection for successive rounds of prime editing. (**a**) Schematic of the strategy for performing successive rounds of coselection. Cells harboring modifications at *ATP1A1* (T804N) and GOI A are first coselected with 0.5 μM ouabain. Following the first round, a subsequent round of coselection occurs at GOI B via modification at *ATP1A1* (Q118R) with 100 μM ouabain. (**b**) PE and indels quantification as determined by BEAT and TIDE analysis from Sanger sequencing. K562 cells harboring the *ATP1A1*-T804N and *RUNX1* +1 ATG insertion (GOI A) modifications were transfected with PE3 vectors targeting *ATP1A1* exon 4 (Q118R) and the indicated GOI B. Genomic DNA was harvested 3 days post-transfection (before selection) and cells were treated (ouabain) or not (untreated) with 100 μM ouabain until all non-resistant cells were eliminated. (**c**) Same as in (**b**) with K562 cells harboring the *ATP1A1*-T804N and *EMX1* +1 G to C (GOI A) modifications. These experiments were performed twice and at different times with equivalent results (see also **Supplementary Fig. 10**).

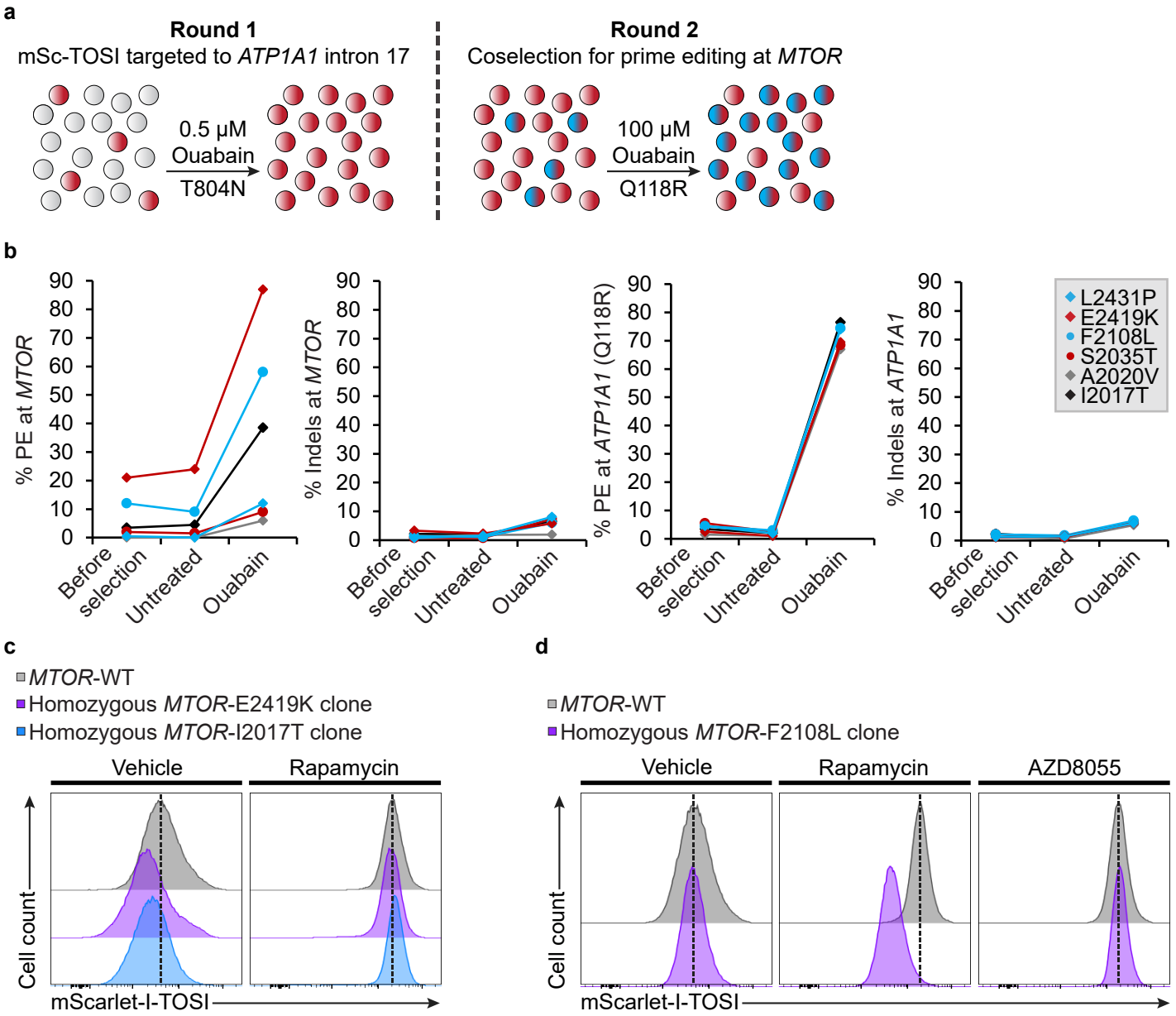
a
Round 1
mSc-TOSI targeted to ATP1A1 intron 17
0.5 μM
Ouabain
T804N
Round 2
Coselection for prime editing at MTOR
100 μM
Ouabain
Q118R
b
% PE at MTOR
% Indels at MTOR
% PE at ATP1A1 (Q118R)
% Indels at ATP1A1
Before selection
Untreated
Ouabain
L2431P
E2419K
F2108L
S2035T
A2020V
I2017T
c
MTOR-WT
Homozygous MTOR-E2419K clone
Homozygous MTOR-I2017T clone
Vehicle
Rapamycin
Cell count
mScarlet-I-TOSI
d
MTOR-WT
Homozygous MTOR-F2108L clone
Vehicle
Rapamycin
AZD8055
Cell count
mScarlet-I-TOSI

Figure 5. Coselection for the installation of clinically relevant mutations at the *MTOR* locus. (**a**) Schematic representation of reporter cell line engineering. K562 cells stably expressing the mSc-TOSI reporter from *ATP1A1* intron 17 are first selected with 0.5 μM ouabain. Then, coselection for PE to insert the indicated mutations at *MTOR* is performed with 100 μM ouabain. (**b**) PE and indels quantification as determined by BEAT and TIDE analysis from Sanger sequencing. K562 cells stably expressing the mSc-TOSI reporter were transfected with PE3 vectors targeting *ATP1A1* exon 4 (Q118R) and *MTOR*. Genomic DNA was harvested 3 days post-transfection (before selection) and cells were treated (ouabain) or not (untreated) with 100 μM ouabain until all non-resistant cells were eliminated. This experiment was performed twice and at different times with equivalent results (see also **Supplementary Fig. 11**). (**c**) Histogram plot of mSc-TOSI intensity in homozygous single cell-derived K562 clones harboring *MTOR* hyperactivating mutations. (**d**) Same as in (**c**) with a homozygous clone harboring the *MTOR*-F2108L rapamycin resistance mutation. Where indicated, cells were treated for 24 hours with 50 nM rapamycin or 50 nM AZD8055 before FACS analysis.